tered and multiply-reflected radiation at the electrodes were exceedingly small compared to the ion currents measured.

In order to compare this method of determining ionization potentials with those mentioned above, a number of molecules were studied and the results are shown in Table I. The accuracy of the values obtained is indicated in the third column, which represents the degree of uncertainty in determining the exact wavelength at which the first ions appear in the measurement of the photoionization current. It is seen that, in general, there is good agreement with those reported by other investigators, exceptionally so with those determined by Rydberg series methods. Since election impact values essentially correspond to vertical processes, it is not surprising that our values are lower and agree better with the more correct spectroscopic values corresponding to adiabatic processes.

An unusual effect was noted in the case of CH_3I and C_2H_5Br. There appeared to be a second threshold at longer wavelengths, although the cutoff was much less pronounced and sharp as compared to the shorter wave length threshold. The ion current was also much smaller than that produced at the shorter wavelength threshold. Two possible explanations for this effect may be given: (1) photoionization of dissociation products which may have lower ionization potentials; or (2) ionization due to transitions $v''>0$ of the ground state of the normal molecule to the $v'=0$ of the ground state of the ionized molecule.

In the case of O_2, NO, NH_3, and CH_3OH, in which no Rydberg series has been observed with any degree of success, it can be seen that the present method is particularly adapted for obtaining accurate measurements of the ionization potential. In fact, this method should be generally applicable for determining first ionization potentials of a wide variety of molecules and in addition for determining molecular ionization cross sections.[2]

PHYSICAL REVIEW VOLUME 91, NUMBER 5 SEPTEMBER 1, 1953

Accurate Determinations of Nuclear Reaction Energies*

K. F. FAMULARO † AND G. C. PHILLIPS
Rice Institute, Houston, Texas

(Received May 29, 1953)

A precise magnetic spectrometer of the annular type is described; the focusing properties and line shapes are analyzed. The use of the instrument to measure absolute particle momenta in terms of the proton magnetic moment precessional frequency and a standard length is presented for three nuclear transmutations and for the determination of the energy necessary to excite a state in Ne^{20}. The Q values obtained are: $C^{12}(d,p)C^{13}$, $Q=2.722\pm0.004$ Mev; $O^{16}(d,\alpha)N^{14}$, $Q=3.119\pm0.005$ Mev; and $Li^7(p,\alpha)He^4$, $Q=17.344\pm0.013$ Mev. The energy at a resonance in the reaction $F^{19}(p,\alpha\gamma)O^{16}$ was determined to be 872.5 ± 1.8 kev.

I. INTRODUCTION

ACCURATE determinations of the energies of evolution of nuclear transmutations yielding heavy particles have been performed in a number of laboratories in recent years; modern techniques have allowed the construction of very precise magnetic and electrostatic spectrometers,[1] and one result of the measurements performed with these instruments has been the preparation of accurate tables of atomic masses for the light elements.[2] A precise knowledge of these masses is desirable so that theories of binding energies of nuclei may be constructed, and to allow the prediction of particle energies and the energies of excitation of nuclei. Atomic masses are also determined with great accuracy by the methods of mass spectrometry; however, it has been pointed out that the nuclear and mass spectroscopic methods have not always yielded mass values that agreed within the assigned errors for the measurements.[2] Since either or both methods could have small errors that might account for this disagreement, it seemed desirable to attempt an accurate, absolute, and independent redetermination of the nuclear data. This paper will describe the techniques developed to accomplish the determinations and will present some of the results.

In reviewing the possibilities of obtaining nuclear disintegration data of greater absolute accuracy than in earlier determinations, five possible sources of error in the previous determinations were noted and an attempt has been made to diminish the magnitude of these possible errors. (1) Most measurements of nuclear transmutation energies have been performed on particles emitted in directions θ that were not optimum with respect to the direction of bombardment. The classical expression for the energy of evolution, Q, of a nuclear

* Supported by the U. S. Atomic Energy Commission.
† Now at the University of Minnesota, Minneapolis, Minnesota.
[1] Buechner, Strait, Stergiopoulos, and Sperduto, Phys. Rev. **74**, 1569 (1948); Snyder, Ruben, Fowler, and Lauritsen, Rev. Sci. Instr. **21**, 852 (1950); Brown, Craig, and Williamson, Rev. Sci. Instr. **22**, 952 (1951).
[2] Li, Whaling, Fowler, and Lauritsen, Phys. Rev. **83**, 512 (1951).

reaction is[3]

$$Q=(M_2+M_3)E_2/M_3-(M_3-M_1)E_1/M_3 -2(M_1M_2E_1E_2)^{\frac{1}{2}}\cos\theta/M_3, \quad (1)$$

where the subscripts 0, 1, 2, 3 refer to the target nucleus, incident particle, produced particle, and the residual nucleus, respectively. Equation (1) may be solved to give

$$E_2^{\frac{1}{2}}=(M_1M_2E_1)^{\frac{1}{2}}\cos\theta/(M_2+M_3) \pm\{M_1M_2E_1\cos^2\theta/(M_2+M_3)^2 +(M_3-M_1)E_1/(M_2+M_3) +M_3Q/(M_2+M_3)\}^{\frac{1}{2}}. \quad (2)$$

Equation (2) shows that $\partial E_2/\partial\theta$ is zero for $\theta=0$, π. In the experiments to be described $\theta=\pi$ and the deviation from $\theta=180°$ is $\pm2°$.

(2) Most previous determinations of nuclear transmutation energies have been measurements relative

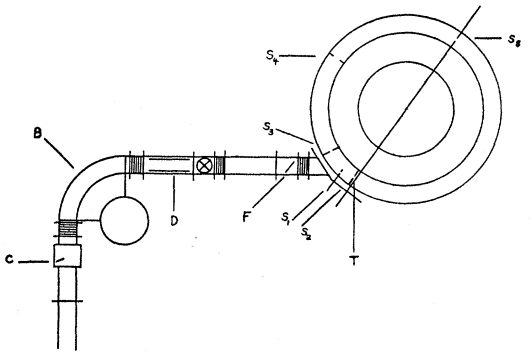

FIG. 1. Experimental arrangement. The accelerated beam is deflected through 90° by the beam analyzing magnet, passes through an auxiliary deflector, and enters the gap of the spectrometer magnet so that its direction is tangent to the mean circle of the spectrometer at the target.

with respect to the older determinations of the natural alpha-particle energies.[4] Although the indications are that the alpha-particle energies are very well known, it seemed desirable to use a more fundamental and independent scale of energies. The scale of energies employed with the Rice spectrometer is derived from the Larmor precessional frequency of the proton magnetic moment in the same magnetic field where the magnetic analysis is performed, and from the radius of curvature as established with a standard meter bar.

(3) Since a particle spectrometer yields a plot of the number of particles *versus* the momentum (or energy), it seemed necessary to develop an objective and fundamental method of assigning a momentum to each group. In the Appendix a simple analysis of the line shapes to be expected from a spectrometer is presented. This knowledge of line shapes has allowed the use of two objective and fundamental methods of assigning momentum.

(4) Because the energy E_2 of the disintegration particles is a function of the bombarding energy E_1, it seemed desirable to use a bombarding energy that could be easily and precisely established, maintained for long periods of time, and monitored frequently. In the experiments to be described the use of a narrow resonance in the $F^{19}(p,\alpha\gamma)O^{16}$ reaction has allowed the bombarding energy to be quickly established.[5] Another proton moment magnetometer in the field of the beam analyzing magnet served to stabilize the magnetic field in the beam analyzer and thus stabilized the energy of the electrostatic generator.

(5) The accumulation of thin surface deposits of contaminants on targets under the conditions of bombardment decreases the energy of the disintegration particles. This difficulty does not meet with any easy, universal solution. Fresh targets, small beam currents, liquid air trapping, and a clean vacuum system have reduced this undesirable effect. Attempts have been made to estimate the thickness of the surface layer by secondary means.

II. APPARATUS

The magnet used for the measurements and the proton moment magnetometer for field stabilization have been described previously.[5] The magnet, of the annular type, has a mean radius of curvature of 35 centimeters, and an annular width of 5 centimeters, although only the central half of the annular region is used. The incident beam from the accelerator is analyzed and then enters the gap of the magnet so that its direction is tangent to the mean circle of the annulus at the target. As shown in Fig. 1, the particles to be analyzed are deflected through 180° of arc and are counted by a detector located diametrically opposite the target.

Magnetic field measurements are made in terms of the Larmor precessional frequency of the magnetic moment of the proton. The stability of the system was such that the field could be held constant to one gauss. The vacuum chamber could be removed from and replaced in the gap of the magnet without disturbing the magnet. This allowed the use of an additional magnetometer to probe the field in the region used to analyze the reaction particles. Nonmagnetic materials were used in constructing the vacuum chamber. A discussion of the method used to correct for small variations of the magnetic field with trajectory arc angle ϕ is given in Appendix A.

The vacuum chamber consists of a two-inch copper tube bent into a semicircle and then flattened. Openings were cut into the chamber, and brass face plates were soldered on to permit the attachment of the beam

[3] M. S. Livingston and H. A. Bethe, Revs. Modern Phys. **9**, 245 (1937). Brown, Snyder, Fowler, and Lauritsen, Phys. Rev. **82**, 159 (1951).

[4] W. B. Lewis and B. V. Bowden, Proc. Roy. Soc. (London) **A145**, 235 (1934); S. Rosenblum and G. Dupouy, Compt. rend. **194**, 1919 (1932).

[5] E. D. Klema and G. C. Phillips, Phys. Rev. **86**, 951 (1952).

entrance port and the insertion of the target assembly at one end and the insertion of the proportional counter detector at the other end.

Comparison of particle group locations before and after removal, disassembly, and replacement of the chamber assured the rigidity and geometrical reproducibility of the system.

The over-all arrangement is shown in Fig. 1. There are five slits in the 180° magnetic analyzer. The beam from the accelerator, after being analyzed by the magnet B (see Fig. 1) and positioned by the electrostatic deflector D, passes through S_1, which is driven by a micrometer screw, then through S_2, and onto the target T. The position of S_1 with respect to S_2 determines the angle at which the beam strikes the target. The slit S_3 prevents particles scattered from S_1 from arriving at the detector. S_4 confines the observed particles to the desired portion of the field. S_5 is in front of the detector and is diametrically opposite to and coplanar with the target.

The width W_c of the detector slit S_5 was about 0.9 mm for most of the measurements while the width W_s of the source was usually determined by the width of S_1 and the geometry of the beam trajectory. Values of W_s ranged from 0.4 mm to 1.4 mm. The incident ion beam was positioned so that when the micrometer position of S_1 was properly placed the beam just grazed the inner edge of S_2. This procedure maintained a constant value $2r_0$ for the distance between the inner edges or source and detector.

The source of proton and deuteron beams for the bombardments was the Rice Institute pressurized Van de Graaff generator.[6] The beam analyzing magnet was monitored with a proton moment apparatus similar to that used with the annular magnet. The stability of the system was such that the spread in bombarding energy due to magnetic field fluctuations and due to the analyzer slit width was no more than ±0.9 kev.

The bombarding energy was determined by means of the resonance at 873.5 kev in the $F^{19}(p,\alpha\gamma)O^{16}$ reaction;[7] thin targets of CaF_2 or ZnF_2, located at C and F in Fig. 1, were used for the calibrations. They were mounted so that they could intercept the beam, or could be rotated aside to let the beam pass. For proton calibration the target at F was used. For deuteron calibration the target at C was positioned to intercept the proton beam from the accelerator, while the molecular hydrogen beam passed through the beam analyzing magnet to give the signal to the electron gun that regulates the generator voltage. This procedure necessitated a correction of +0.7 kev for the difference of mass of H_2^+ and D^+ ions.

Since the beam analyzing magnet and the annular magnet were separated by a distance of about one meter, their fields interacted slightly. Hence, the energy calibration of the generator was always performed with the field of the annular magnet held at the field that was to be used for the bombardment.

TABLE I. Scattering of 873.5-kev protons from a 34 μg/cm² Au target for various widths and positions of openings of the slit $S4$ located at 90° of trajectory arc.

Width of slit S_4 (inches)	Displacement (inches) of the center of the opening at S_4 relative to the mean circle of the annulus. (+out, −in)	Intercept of tangent Mc/sec	Width at half-maximum Mc/sec
¼	−⅜	16.290	0.047
¼	−⅛	16.303	0.049
¼	+⅛	16.332	0.046
¼	+⅜	16.302	0.047
¼	−⅜	16.300	0.047
¼	−⅛	16.306	0.043
¼	+⅛	16.291	0.043
¼	+⅜	16.295	0.050
1	0	16.294	0.050
1½	0	16.294	0.052
2	0	16.306	0.055

III. THE ASSIGNMENT OF MOMENTUM TO PARTICLE GROUPS

Since the particle momenta were to be assigned from a knowledge of the radius of curvature in the magnetic

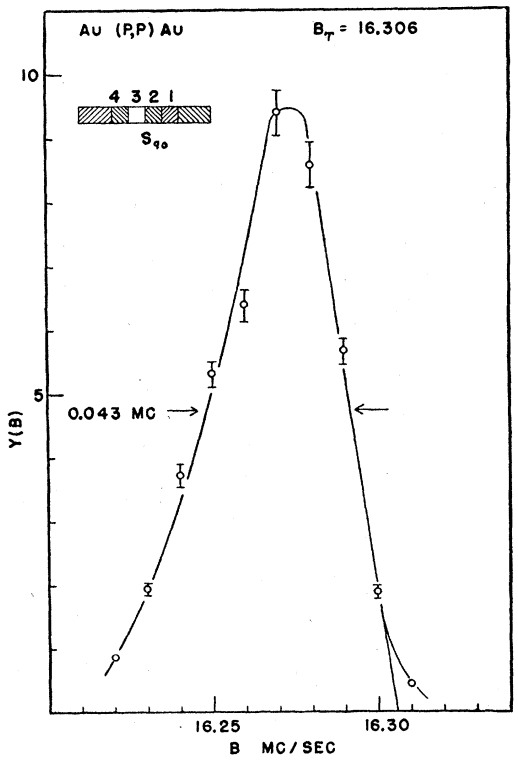

FIG. 2. Proton counting rate *versus* magnetic field for protons elastically scattered by a 34 μg/cm² evaporated Au layer. The energy of the scattered protons is about 855 kev.

[6] Bennett, Bonner, Mandeville, and Watt, Phys. Rev. **70**, 882 (1946); S. J. Bame, Jr., and L. M. Baggett, Rev. Sci. Instr. **20**, 839 (1949); B. E. Watt, Rev. Sci. Instr. **17**, 334 (1946).

[7] Herb, Snowdon, and Sala, Phys. Rev. **75**, 246 (1949).

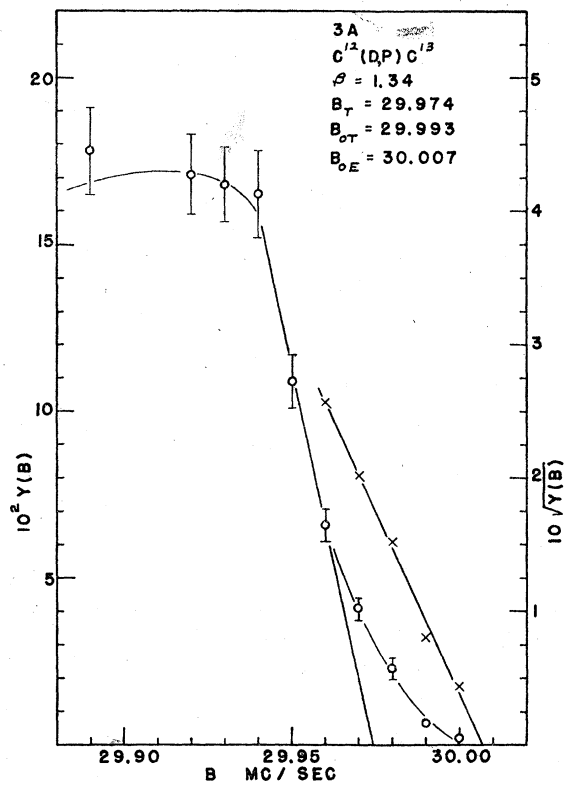

FIG. 3. Proton counting rate *versus* magnetic field for protons from $C^{12}(d, p)C^{13}$ (thick target).

field, it was necessary to develop criteria for this assignment and to understand the focusing properties of the spectrometer. The focusing characteristics of the field were investigated by the scattering of protons, whose energy was standardized with the 873-kev resonance of the $F^{19}(p, \alpha\gamma)O^{16}$ reaction. The target was a thin layer (34 μg/cm^2) of gold evaporated onto an aluminum foil. A typical counting rate *versus* magnetic field curve is shown in Fig. 2. Between successive bombardments the slit S_4 at the trajectory arc angle $\phi = 90°$ was changed in position and width, so that the focusing properties of each part of the field could be observed. In Table I are recorded the widths at half-maxiumm of the peaks, and the intercept, B_T, of the tangent to the peak on the high momentum side. When more than the central one-half of the annulus was open at $\phi = 90°$, it was observed that the peaks developed tails on both sides, and that the peak counting rates did not increase proportional to the solid angle. For this reason the slit S_4 was permanently set so that just the central half of the annulus was open. The intercept, B_T, obtained from the data using different one-quarter inch fractional apertures of the central one inch of the annulus were as consistent as it was possible to reset and maintain the incident proton energy. The spread of ± 0.008 Mc/sec (excluding one bombardment) corresponds to a variation of the generator voltage of ± 0.9 kev. The widths of the peaks agreed with that expected from the thickness of the target, and source size and detector slit width.

Thus, it was concluded that the extrapolated end point was a reliable measure of the particle momenta, and further that this end point did not vary over the particle trajectories in the usable region of the annulus. The observations implied that, to the limits of our ability to discern, the spectrometer acted as an ideally focusing instrument; a line should be focused to a line. Hence, it seemed reasonable to assign as the radius of curvature, r_0, one-half the distance between the inner edges of the slits S_2 and S_5. This distance is the natural one that arises in the analysis of line shapes for an ideally focusing instrument and is the radius of curvature of the first particles to be detected when the magnetic field, initially too large, is lowered to allow the group to enter the detector. The Appendix B discusses the analysis of line shapes.

The shape of lines to be expected from thick targets indicated that the lower part of the high momentum edge is parabolic and that, if the square root of each datum point in this region is plotted, the intercept, B_{0E}, of the resulting straight line is the magnetic field corresponding to r_0. The analysis also indicated that the tangent at half-maximum to the group on the high-momentum side possesses an intercept, B_T, that when appropriately corrected upwards corresponds to r_0 also.

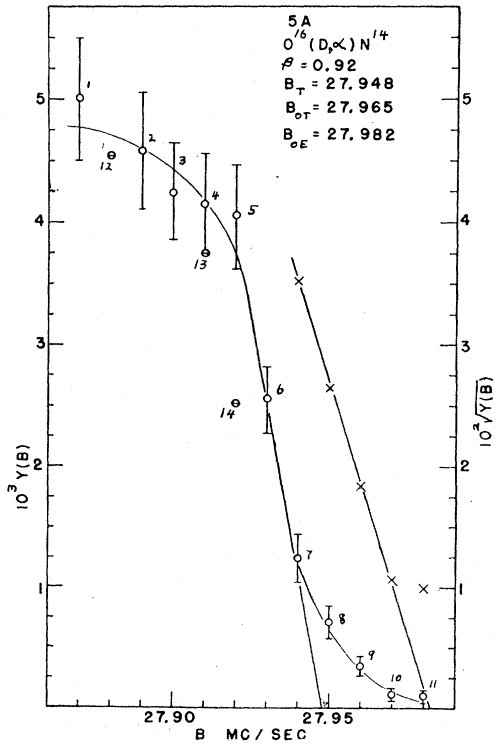

FIG. 4. Alpha counting rate *versus* magnetic field for alpha particles from $O^{16}(d, \alpha)N^{14}$. Points plotted as θ's were taken last and show the shift due to formation of carbon contamination.

Both of these methods were used for the $C^{12}(d, p)C^{13}$ reaction and gave satisfactory agreement. When thin targets were used, the tangent to the linear part of the high momentum edge of the peak was extended to zero counting rate, and the intercept, B_T, corrected upwards to obtain the true magnetic field, B_{0T}.

IV. RESULTS

The measurements of the Q values for three nuclear reactions are discussed below, along with a description of an absolute determination of the resonant energy of a level in Ne^{20} excited by the $F^{19}(p, \alpha\gamma)O^{16}$ reaction.

$C^{12}(d, p)C^{13}$

Altogether, eight determinations were made on the particles from this reaction. The corrected extrapolated end points appeared to be independent of the source width and the thickness of the target and thus lent credence to the line shape analysis. In order to test the validity of corrections to the field necessitated by small field variations along the trajectory arc angle ϕ, the magnet was reshimmed so that the correction changed in magnitude and sign. The corrected end points before and after shimming showed satisfactory agreement. This reaction also served to monitor the rigidity of the system, by determining the location of the proton group before and after the determination of the other reactions. Since the maximum yield from a thick target of carbon bombarded by deuterons was well established by these measurements, it was then possible to determine quickly the amount of carbon that had accumulated on other targets by observing the $C^{12}(d, p)C^{13}$ maximum yield. This procedure only required a few minutes of bombardment.

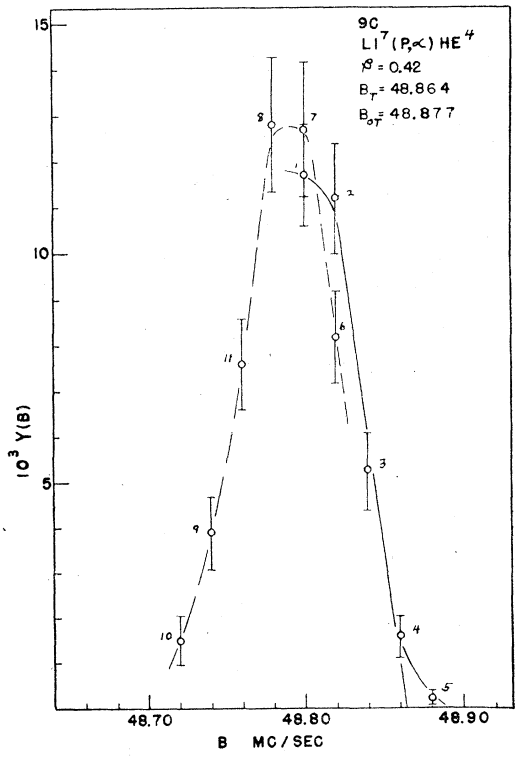

FIG. 5. Alpha counting rate *versus* magnetic field for alpha particles from $Li^7(p, \alpha)He^4$. The high momentum edge was first obtained. The remainder of the curve (dashed) shows effect of carbon contamination layer.

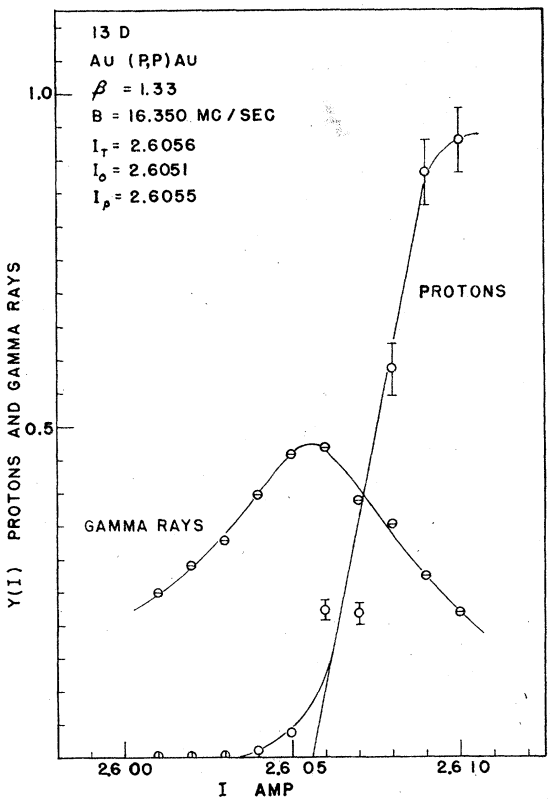

FIG. 6. Determination of the 873.5-kev gamma-ray resonance in $F^{19}(p, \alpha\gamma)O^{16}$. The spectrometer field was held constant and the bombarding energy varied. Circles are the scattered protons; the points, θ, are the gamma rays.

Typical thick target data, with the square root of the parabolic tail plotted, and with the tangent at half-maximum constructed, is shown in Fig. 3.

$O^{16}(d, \alpha)N^{14}$

Thick targets of copper oxide were used, and the data for one measurement are shown in Fig. 4. The corrections for carbon contamination, as discussed above, applied to E_1 and E_2 were -1.8 kev and $+5.0$ kev, respectively. The yield from this reaction is relatively weak and necessitated long bombardments and the consequent accumulation of the carbon layer. The data points plotted as θ show the downward shift that the particles momenta suffered due to the surface layer.

$Li^7(p, \alpha)He^4$

The targets for these experiments consisted of 60 $\mu g/cm^2$ of LiF evaporated onto 0.2 mg/cm^2 aluminum foils. The data of one bombardment are shown in Fig. 5. The carbon contamination corrections applied to E_1 and E_2 were -1.2 kev and $+2.6$ kev, respectively.

$Au(p, p)Au$

A redetermination of the position of the 873.5-kev resonance in $F^{19}(p, \alpha\gamma)O^{16}$ was made by the scattering of protons from a 5 $\mu g/cm^2$ gold layer evaporated on an aluminum foil. One determination was obtained by setting the energy of the proton beam at the peak of the gamma-ray resonance and then varying the field of the spectrometer to obtain the momentum of the scattered proton group. The second method consisted of varying the energy of the incident protons while the field in the spectrometer was held constant. At each energy the proton beam was first intercepted by a thin CaF_2 target and the gamma-ray yield from the target recorded, and then the beam was passed into the spectrometer and the yield of scattered protons recorded. These data are shown in Fig. 6. Corrections for the thickness of the CaF_2 target were determined by comaprison with a very thin target. No carbon contamination correction was applied to the data, but an error of 1 kev was assigned for this possibility.

A summary of these measurements and their assigned errors is presented in Table II. The Q values, calculated as is indicated in Appendix C, are also tabulated for the three transmutations, while for the gold scattering the Q value must be zero and so the bombarding energy at resonance can be calculated.

CONCLUSIONS

The energy values determined from these measurements are compared with other recent precise determinations in Table III. It is seen that in all of the cases the agreement is rather close.

In the case of the $C^{12}(d, p)C^{13}$ reaction the Q value of this report falls about at the mean of the two previous determinations,[5,8] which had shown a realtively large dispersion.

For the $Li^7(p, \alpha)He^4$ and the $O^{16}(d, \alpha)N^{14}$ reactions the Q values of this experiment overlap in probable errors with the previous accurate measurements,[8–10] while the redetermination of the resonance enregy of the 873-kev for the $F^{19}(p, \alpha\gamma)O^{16}$ reaction agrees reasonably well with the earlier standard.[7]

Thus, it can be concluded that the results of these experiments have not revealed any errors in the natural alpha-particle energy scale,[4] nor in the electrostatic energy scales.[7,9]

As an example of the disagreement that remains between nuclear and mass-spectroscopic mass values, we

TABLE II. A summary of the measurements of the three nuclear reactions and the resonant energy determination experiment.

Experiment No.	Reaction	Extrapolated end point Mc/sec: From square root plot	Extrapolated end point Mc/sec: From correction of intercept of tangent	Extrapolated end point Mc/sec: Mean	Field correction Mc/sec	Final end point Mc/sec	Bombarding energy before contamination correction Mev
1	$C^{12}(d, p)C^{13}$		29.995	29.995	+0.065	30.060	0.8755
2			29.990	29.990	+0.065	30.055	0.8747
3		30.007	29.993	30.000	+0.065	30.065	0.8760
4			29.995	29.995	+0.065	30.060	0.8769
6			29.996	29.996	+0.065	30.061	0.8778
7		29.995	29.998	29.996	+0.065	30.061	0.8782
11		30.081	30.080	30.080	−0.019	30.061	0.8767
						30.060	0.8765
						±0.005	±0.0023
						Mean	Mean
5	$O^{16}(d, \alpha)N^{14}$	27.982	27.965	27.973	+0.061	28.034	0.879
						±0.008	±0.002
9	$Li^7(p, \alpha)He^4$		48.887	48.877	−0.005	48.872	0.8758
10			48.881	48.881	−0.005	48.876	0.8758
						48.874	0.8758
						±0.005	±0.0014
						Mean	Mean
12	$Au(p, p)Au$		16.357	16.357	−0.013	16.344	
13			16.352	16.352	−0.013	16.339	
						16.341	
						±0.005	
						Mean	

[8] Strait, Van Patter, Buechner, and Sperduto, Phys. Rev. **81**, 747 (1951).
[9] Craig, Donahue, and Jones, Phys. Rev. **88**, 808 (1952).
[10] Collins, McKenzie, and Ramm, Proc. Roy. Soc. **A216**, 242 (1953).

have calculated the mass of N^{14}. To do this one must assume masses for the deuteron and alpha particle. The values given by Li, Whaling, Fowler, and Lauritsen[2] have been used. The mass obtained for N^{14} is 14.07512 ($\pm$11) amu, while Nier[11] gives 14.007564 ($\pm$7) amu. These masses differ by 46 kev, which is considerably outside the errors assigned to the two determinations.

The redeterminations of the Q values with the Rice spectrometer are being continued.

The authors wish to thank Professor T. W. Bonner for his continued encouragement and advice. We wish to thank Mr. J. F. Vander Henst and Mr. Earl J. Harmening for construction of the vacuum tube, and Mr. C. R. Gossett for aid in operation of the accelerator and spectrometer.

APPENDIX A. MAGNETIC FIELD CORRECTIONS

At the conclusion of the measurements determining the magnetic rigidity of a particle group, the variation

TABLE III. Q values reported in this work compared with other determinations.

	This report Mev	Previous determinations Mev
$C^{12}(d, p)C^{13}$	2.722±0.004	2.716±0.005[8] 2.732±0.006[5]
$O^{16}(d, \alpha)N^{14}$	3.119±0.005	3.112±0.006[8] 3.119±0.005[2] 3.113±0.003[9]
$Li^{7}(p, \alpha)He^{4}$	17.344±0.013	17.340±0.014[8] 17.338±0.011[2] 17.352±0.009[10]
$F^{19}(p, \alpha\gamma)O^{16}$ resonance	0.8725±0.0018	0.8735±0.0009[7]

of the magnetic field with the trajectory arc angle ϕ was investigated. The vacuum tube was removed from the annular gap of the magnet and a proton moment magnetometer was used to measure these variations with respect to the magnetometer that regulated the magnetic field. The measurements were carried out with both the 180° magnetic spectrometer and the beam analyzing magnet at the field strengths used in the preceding experiments. A typical result of such a measurement is shown in Fig. 7.

The correction δB, to the observed field, $B(0)$, at the source, necessary to give the effective field was that given by Hartree:[12]

$$\delta B=\tfrac{1}{2}\int_0^{\pi}\Delta B(\phi)\,\sin\phi d\phi,$$

where $\Delta B(\phi)=B(\phi)-B(0)$.

[11] A. O. Nier, Phys. Rev. **81**, 624 (1951).
[12] D. R. Hartree, Proc. Cambridge Phil. Soc. **21**, 746 (1923).

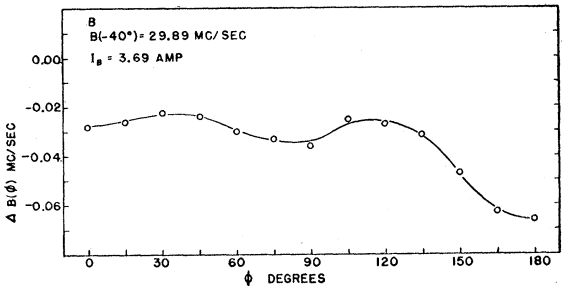

FIG. 7. The deviation of magnetic field strength, expressed in Mc/sec, *versus* the trajectory arc angle ϕ, measured from the target position.

APPENDIX B. LINE SHAPE ANALYSIS

The results of the scattering of protons from gold as performed in the Rice spectrometer indicated that: (1) the central one-half of the available solid angle produces a group whose extrapolated end point was a reproducible relative measure of the particle momentum (2) the line width was entirely explicable as due to the source and detector slit widths. The facts presented in Sec. III indicated that to a good approximation the spectrometer acted as a perfect focusing one; it acted as though it focused a line source of monoenergetic particles to a line. If this is assumed and if it is also assumed that the source emits equal numbers of particles per unit momentum interval, and that the momentum loss of particles produced in a thick target is proportional to the depth in the target, then one may derive a simple theory of the line shape to be expected.

The symbols are defined as:

W_s, W_c are the widths of the source and detector slits, respectively.
h is the height of the slits.
σ is the cross section for the reaction $\times N$, the number of atoms/cm^3, $\times 1/e$, where e is the electronic charge in μ coulombs.
Ω is the acceptance solid angle of the spectrometer.
P_0 is the momentum of particles originating at the surface of the target.
k_1 and k_2 are the stopping cross sections for the incident and observed particles in the target material.
ρ_0 is the radius of curvature of particles with momentum P_0 in a magnetic field B.
a is defined by $P_0=aB\rho_0$, so that $a=Ze/\gamma$.
$p(\eta)$ is the observed momentum of particles originating at a depth η in the target is $P_0-p(\eta)$, where $p(\eta)=(NP_0/2E_2)\times(k_1\partial E_2/\partial E_1+k_2)\eta$ and C is a constant defined by the equation $p(\eta)=C\eta$.
x is the coordinate of a point in the focal plane.
r_0 is one-half the distance from the inner edges of the source and detector slits.

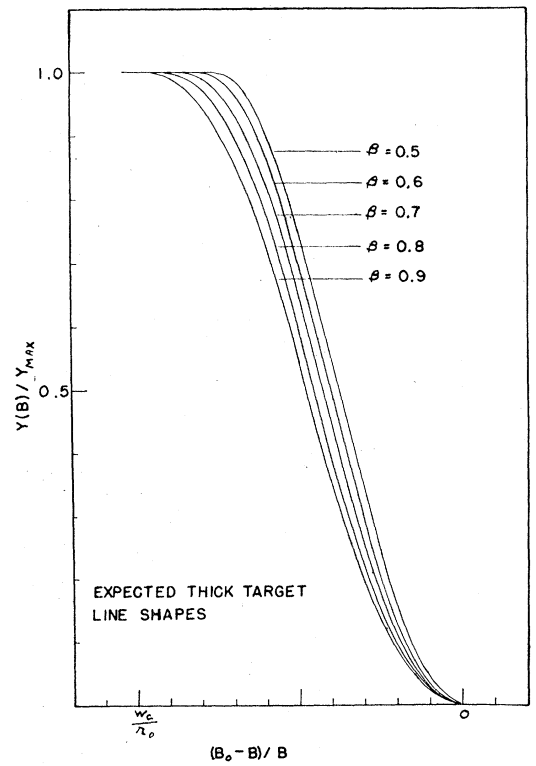

FIG. 8. Expected thick target line shapes. The ratio, $Y(B)/Y_{\max}$, of yield to maximum yield is plotted *versus* the normalized magnetic field strength $(B_0-B)/B$, where B is the magnetic field and (B_0-B) is the deviation from the end-point field B_0. Curves for various values of the ratio, $\beta=W_s/W_c$, of the source to list widths are presented.

The particles originating in a volume element $d\tau=hW_s d\eta$ in the target are focused into a rectangular intensity distribution $n(x,\rho_0)d\eta$ in the focal plane, where

$$n(x,\rho_0)=(\Omega\sigma/W_s)$$

for

$$2\rho_0(1-p(\eta)/P_0)-W_s\leqslant x\leqslant 2\rho_0(1-p(\eta)/P_0)$$

and $n(x,\rho_0)=0$ otherwise.

The number arriving at x in dx is

$$N(x,\rho_0)=\int_{\eta_1}^{\eta_2} n(x,\rho_0)d\eta.$$

Then for $W_s\geqslant 2\rho_0-x$, $\eta_1=0$ and $\eta_2=(P_0/2C\rho_0)(2\rho_0-x)$, while for $W_s\leqslant 2\rho_0-x$, $\eta_2-\eta_1=P_0W_s/2C\rho_0$. Thus

$N(x,\rho_0)=(\Omega\sigma aB/2CW_s)(2\rho_0-x)$ for $0\leqslant 2\rho_0-x\leqslant W_s$;

$N(x,\rho_0)=(\Omega\sigma aB/2C)$ for $2\rho_0-x\geqslant W_s$.

The number of particles that enter the detector slit is then given by:

$$Y(B)=(ABr_0^2/W_s)[(B_0-B)/B]^2 \quad \text{for } 0\leqslant(B_0-B)/B\leqslant W_s/2r_0;$$

$$Y(B)=ABr_0[(B_0-B)/B-W_s/4r_0] \quad \text{for } W_s/2r_0\leqslant(B_0-B)/B\leqslant W_c/2r_0;$$

$$Y(B)=(ABr_0^2/W_s)\{W_sW_c/2r_0^2-[(B-B_0)/B-(W_s+W_c)/2r_0]^2\} \quad \text{for } W_c/2r_0\leqslant(B_0-B)/B\leqslant(W_s+W_c)/2r_0;$$

$$Y(B)=ABW_c/2 \quad \text{for} \quad (W_s+W_c)/2r_0\leqslant(B_0-B)/B;$$

where $A=\Omega\sigma a/C$ and $W_s<W_c$. Similar expression may be obtained for $W_s>W_c$. Typical thick target line shapes are shown in Fig. 8 for $W_s<W_c$.

Two facts are to be noted from this analysis: (1) the high momentum edge of the line is parabolic, and if the square root of the experimental $Y(B)$ is plotted in this region, then the true end point B_0 is the intercept of the resulting straight line with the abscissa. (2) The line at half-maximum is linear and an extrapolation of this line to the abscissa, corrected upwards by the factor $(1+W_s/4r_0)$ for $W_s<W_c$ and $(1+W_c/4r_0)$ for $W_s>W_c$, will yield the same true end point B_0.

Thin target curves may be easily obtained by subtracting two thick target curves where one curve is displaced by a distance in the focal plane given by

$$\delta=(r_0\Delta E_1/E_2)(\partial E_2/\partial E_1+k_2/k_1).$$

The resultant distributions are triangular or trapezoidal, and when integrated over the finite detector slit width, various types of line shapes are obtained. One can easily see, however, that there will again be a linear portion to the high momentum edge of the line and the intercept of this may be corrected, upwards to give the true end point. The correction factors are $(1+\delta/4r_0)$ for $\delta<W_s$, $W_s<W_c$, and $(1+W_s/4r_0)$ for $W_s<\delta$, $W_s<W_c$.

APPENDIX C. CALCULATION OF Q VALUES

The equations used for computing the Q values were[3]

$$Q=E_2+E_3-E_1,$$

and since the observation angle $\theta=\pi$ the momenta obey the scalar relations

$$P_3=P_1+P_2.$$

The spectrometer measures the nonrelativistic energy $P_2^2/2M_2$, where

$$(2\pi^2Z_2^2/10^{14}\gamma_p^2)(M_p/M_2)(e/M_p)B_0^2r_0^2=P_2^2/M_2,$$

and this energy is related to the relativistic energy by

$$E=P^2/2M-E^2/2MC^2.$$

We have used $\gamma_p=(2.67523\pm0.00006)\times10^4$ sec^{-1} gauss^{-1}, and $e/M_p=(9579.4\pm0.3)$ emu/g.[13,14]

In the above formula P_2, M_2, and Z_2 are the momentum, mass, and charge number of the analyzed particles, while r_0 is one-half the distance in centimeters between the inside edge of the source and the inside edge of the detector slit. B_0 is the corrected end point of the line expressed in mc/sec. Nuclear masses were used in the calculations.[2]

[13] Summer, Thomas, and Hipple, Phys. Rev. **82**, 697 (1951).
[14] J. W. M. DuMond and E. R. Cohen, Phys. Rev. **82**, 555 (1951).